Volume 1 | Number 1 | Jan 2013 | Pages 1–100

Journal of
Materials Chemistry B

Materials for biology and medicine
www.rsc.org/materialsB

ROYAL SOCIETY
OF CHEMISTRY

ROYAL SOCIETY
OF CHEMISTRY

www.rsc.org/materialsB

Journal of Materials Chemistry B

Gelatin-Poly(vinyl alcohol) Porous Biocomposites Reinforced with Graphene Oxide as Biomaterials

M. Ionita[a], L. E. Crica*[a], H. Tiainen[b], H. J. Haugen[b], E. Vasile[a], S. Dinescu[c], M. Costache[c], H. Iovu[a]

The present work aims to develop new biocomposites based on gelatin (Gel) and poly(vinyl alcohol) (PVA) reinforced with graphene oxide (GO). On the one hand, the model is designed by consideration of the high performance of the aforementioned biopolymers as biomaterials; on the other hand, the original component of the system – GO, is expected to improve structural stability and boost mechanical strength. Porous Gel – PVA / GO materials with GO 0.5 to 3 t.% by weight are obtained by freeze-drying. Structural analysis by Fourier Transform Infrared spectrometry (FT-IR), X-ray diffraction (XRD) and transmission electron microscopy (TEM) revealed the ability of well-dispersed GO nanosheets to set interactions with the polymers, leading to a unique molecular structuration. 3D analysis by X-ray microtomography (microCT) and scanning electron microscopy (SEM) suggests the influence of GO on pores adjustment. According to mechanical tests, GO undoubtedly exhibits a beneficial effect on polymers resistance against compressive stress, improving their compressive strengths by 97 – 100 % with the addition of 0.5 – 3 wt.% GO. Moreover, biological assessments using the MC3T3-E1 preosteoblast murine cells line indicated the fabrication of a cytocompatible composite formula, with potential for further *in vivo* testing and tissue engineering applications.

Introduction

Taking a survey of biomaterials evolution, one can remark upon the leap from external simple prostheses and devices to more complex internal biodegradable implants. If decades ago the loss of a body part was usually followed by defective healing, nowadays improved standard therapy conditions and prosthetics are paving the way for regenerative medicine. While tissue grafts derived from different donors are compromised by immunogenicity issues, new readily available biocompatible materials with suitable physical, chemical and biological innate properties are required.[1] The development of biomaterials based on neat or combined organic and inorganic compounds, loaded with drugs, genes, growth factors or nutrients are currently the focus of much ongoing research. Such non-self-structures must fit implantation sites and be stable towards internal conditions such as pH, temperature, degradative media and mechanical stress. Hand in hand with biomolecular permittivity, the capacity to sustain cellular activities and promote angiogenesis are now considered additional key-factor for regenerative processes.[2, 3] Such biomaterials must mimic the native tissue media as close as possible and encourage neotissue formation.[1]

Amongst the broad range of biomaterials, polymers are a class that share similarities with natural tissues, mostly in terms of physico-chemical nature, therefore they are often preferred as tissue regeneration biomaterials. Collagen, a trihelical organized polymer, is the predominant protein found within human structures.[4] Often extracted from bovine and porcine sources, it nonetheless exhibits major drawbacks as a natural biomaterial, such as a high rate of immune reactions, as well as inadequate mechanical performances for applications such as vascular or hard tissue engineering.[5, 6] By collagen hydrolysis, collagen chains are detangled and a non-immunogenic derivative called gelatin (Gel) is obtained,[5] which is often preferred as an alternative to its precursor. However, its mechanical behavior is further compromised and thus Gel is often mixed with various organic and inorganic reinforcing agents. For instance, *Mozafari et al.* used bioactive glass (BaG) to reinforce gelatin nanocomposite scaffolds and reported a compressive yield strength of 5.6 MPa for a 10 wt.% BaG nanoparticles, getting close to the values of natural spongy bone.[7] Another study indicated the use of silk fibers to increase tensile strength and modulus by 259 and 400 %, respectively,[8] while the addition of some inorganic compounds such as zirconium oxide nanoparticles seems to weaken Gel mechanical resistance due to the absence of favorable interfacial interactions.[9] Titanium oxide is capable to double the compressive strength of Gel-hydroxyapatite biocomposite scaffold, under a hydroxyapatite : titania : gelatin weight ratio of 1 : 2 : 2.[10] Aside from natural biopolymers, synthetic polymers are reliable alternative options within the biomaterials field. This is a result of their high availability and absence of immunogenic sites from their structures, while they are easy to

a. *Advanced Polymer Materials Group, University Politehnica of Bucharest, Gh. Polizu 1-7, Bucharest 011061, Romania. *E-mail: liviaec@mail.uio.no*

b. *Department of Biomaterials, Institute for Clinical Dentistry, University of Oslo, P.O. Box 1109 Blindern, NO-0317 Oslo, Norway.*

c. *Department of Biochemistry and Molecular Biology, University of Bucharest, Bucharest 050095, Romania.*

handle and have adjustable biodegradability. Poly(vinyl alcohol), a water-soluble polymer, is one of the most popular polymers used in biomedicine, currently used for commercial contact lenses, surgical absorbents and disposable bags in hospitals, and trialed for the development of wound dressing hydrogels and tissue regeneration scaffolds.[11, 12] On account of its generous properties such as biocompatibility and ability to form stable hydrophilic networks, it is favoured for the development of tissue regeneration biomaterials.[13] Numerous studies highlight its potential to support *in vitro* and *in vivo* cellular activities, both *per se* and in combinations with other chemical compounds.[14, 15] For instance, when combined with Gel and freeze-dried, highly porous biocomposite scaffolds are obtained. Such architectures can offer a tridimensional environment in which cells are able to live, develop and proliferate.[16] Accordingly, the interconnected pores should support the in-diffusion of signal molecules, growth factors and nutrients, as well as the out-diffusion of waste products.[16] In addition, there is still a need for improved mechanical resistance in such materials, especially when aiming for hard tissue therapy. While previous examples of reinforcing agents did not seem to match ideal requirements, new types of graphene-based reinforcers offering improved mechanical and biological performance are currently showing up in the spotlight.[17-20] Among these, graphene oxide (GO) has markedly valuable versatile chemistry, with numerous reactive oxygenated functionalities such as –OH, -COOH and -C-O-C-, which support nanosheets dispersion in aqueous media and facilitate chemical interactions with polymers.[21] On the one hand, GO incorporation within polymeric matrix is also proficient in enhancing biopolymers resistance against both compressive and tensile stress.[18, 22, 23] On the other hand, even though the mechanism by which carbon-based materials improve biological activities is not fully clarified so far, such materials are indicated to enhance cells attachment, viability and proliferation and maintain the capacity to induce stem cells differentiation into adipose, cartilage and bone cells.[24-26] Notably, recent studies demonstrate the anti-cancer potential of GO against a wide range of cancer stem cells types, from breast, ovarian and prostate tumors to lung, pancreatic and brain cancer cells.[27]

On the basis of these aforementioned facts, we sought synthesis and characterization of a ternary biodegradable porous composite of Gel, PVA and GO (Gel – PVA / GO), with different GO concentrations (0.5 to 3 wt.%). On the one hand, Gel is highly soluble in water and thus PVA was used to achieve a more chemically stable composition against water-based media. On the other hand, the materials underwent an adapted treatment of cyclic freeze-thawing in order to release internal tensions caused by ice crystals growth during freezing,[28, 29] such cyclic treatments being well-known to be used for PVA physical cross-linking as well.[13] Nevertheless, given the previously enumerated advantages of graphene based materials, we aimed to boost mechanical resistance and facilitate cellular activities through the use of GO. Therefore, our porous Gel – PVA / GO biocomposites were expected to meet the requirements of improved mechanical behavior and proper

biomaterial-cells interactions. In this regard, materials structuration was evaluated by Fourier Transform Infrared spectrometry (FT-IR), X-ray diffraction (XRD) and transmission electron microscopy (TEM), followed by tridimensional analysis (3D analysis) by X-ray microtomography (microCT) and morphological studies by scanning electron microscopy (SEM). Subsequently, mechanical behavior against compressive stress was determined, while materials biocompatibility was evaluated in terms of cytotoxicity and cells viability.

Experimental

Chemicals and reagents

Graphene oxide used for biomaterials synthesis was purchased from National Institute for Research and Development in Microtechnologies (Romania) and prepared according to Hummers method.[30] In addition, cold water fish skin gelatin (solid BioReagent, 60 kDa MW) and poly(vinyl alcohol) (130000 g / mol MW, +99 % hydrolyzed) from Sigma Aldrich (USA) were used for the polymeric matrix composition.

Materials used for samples preparation for microCT scanning were iodine (Fluka, iodide purum p.a., ≥99.5% at RT) and hexa(methyl disilazane) (reagent grade, ≥99%) from Sigma Aldrich (USA), while absolute ethanol was purchased from Kemetyl Norge (Norway).

Dulbecco's modified Eagle's medium (DMEM) (Sigma-Aldrich, Steinheim, Germany) and fetal bovine serum (FBS) (Life Technologies, Foster City, CA) were used for cell cultures, while 3-(4,5-dimethylthiazol-2-yl)-2,5-diphenyltetrazolium bromide (MTT) and In Vitro Toxicology Assay Kit, Lactic Dehydrogenase (LDH) based (Sigma-Aldrich, Steinheim, Germany) were used for biocompatibility tests. All chemicals were used without additional purification.

Gel – PVA / GO biocomposites synthesis

Gel – PVA / GO biocomposites with 0.5, 1, 2 and 3 wt.% GO were prepared by a simple protocol followed by freeze-drying. The protocol was initiated by dispersing each amount of GO through ultrasound (US) treatment in 25 mL distilled water for 1 hour, in an ice bath. Thereafter, Gel flakes were added in portions under constant stirring at 60 °C, for the preparation of a 5 wt.% solution. 5 wt.% PVA solution was prepared by dissolving polymer pellets in distilled water by 1 hour autoclaving at 120 °C. A volume of 25 mL of the obtained 5 wt.% PVA solution was next added to each Gel / GO solution previously prepared. The mixtures were US treated once again for 30 minutes, in the same conditions as above.

The well homogenized Gel - PVA / GO composite solutions were poured on transparent Petri dishes and frozen at -70 °C overnight. Subsequently, each sample was subjected to a 3-cycles treatment consisting of room temperature melting for 3 hours and refreezing at -70 °C for 21 hours, in order to stabilize composites structures. Samples in their final state were obtained by freeze-drying for 2 days.

Sonication was performed using a VCX750 ultrasonic processor for small and medium volume applications from Sonics & Materials, Inc. (53 Church Hill Road, Newton, CT 06470-

1614 USA) equipped with a titanium alloy (Ti-6Al-4V) probe tip and a 750 W source operating at a frequency of 20 kHz. The probe tip vibrations were set to 80 % amplitude and sonication time was chosen to be 1 hour for GO dispersion in water and 30 minutes for Gel - PVA / GO solution. In order to avoid samples alteration due to overheating during sonication, mixtures were kept at low temperature in an ice bath.

Lyophilisation was performed at -50 °C and 0.040 mbar, using a Christ LCG Alpha 2-4 LD plus laboratory freeze-dryer equipped with a PMMA chamber (Martin Christ, Gefriertrocknungsanlagen GmbH, Postfach 1713, 37507 Osterode am Harz).

Characterization techniques

FT-IR

Composites structural features were primarily evaluated by Fourier transform infrared (FT-IR) measurements, using a Spectrum 400 FT-IR/FT-NIR Spectrometer from PerkinElmer, UK. The wavenumber range was set to 650 - 4000 cm^{-1} with a resolution of 4 cm^{-1} and the spectra output was displayed in absorbance. Bands identification was done using SpectrumIMAGE dedicated software.

XRD

X-ray diffraction analysis (XRD) was done at room temperature using a Panalytical XPert Pro MPD instrument equipped with CuKα radiation source of 1.54065 Å wavelength. Reported diffractograms were recorded in the 2 theta range of 5 to 50 ° and intensities are displayed in arbitrary units (a.u.). For each sample, the values of interlayer spacing d were calculated from *Bragg*'s law:[31]

$$n\lambda = 2\,d\,\sin\theta, \tag{1}$$

where n is the reflection order, λ is the X-ray wavelength and ϑ is the diffraction angle.

The mean size of the ordered domains τ was calculated according to *Scherrer* equation:[32]

$$\tau = \mathrm{K}\,\lambda\,/\,\beta\,\cos\theta, \tag{2}$$

where K is the shape factor (constant) and β is the full width at half maximum (FWHM).

TEM imaging

Materials structure chemical fixation was the first stage in samples preparation for TEM investigation. For each sample, specimens of 1 mm³ were immersed for 2 hours in a prefixation aqueous buffer solution containing sodium cacodylate, calcium chloride and glutaraldehyde. Before and after subjecting the samples to the osmium tetroxide (OsO_4) fixative solution, a triple washing with mixtures of sodium cacodylate buffer, sucrose and distilled water was performed. Further on, samples were dehydrated by multiple immersions in concentrated acetone solutions. The next step was embedding in Epon 812-based liquid resin, followed by polymerizing for 48 hours at 60 °C before ultramicrotome cutting. Eventually, cut samples were collected on metal mesh "grids" and stained by "double contrasting". This implied contacting the grids with uranyl acetate solution for 8 minutes, washing them 2 times with 50 % acetone solution followed by distilled water and drying with filter paper. Next, the grids were placed on drops of lead citrate inside a Petri dish and few sodium hydroxide pellets were added to absorb the water vapors. After 11 minutes, the grids were rinsed with water several times and eventually dried on filter paper.

Subsequently, samples were imaged using a TECNAI F30 G²S Twin High Resolution TEM equipment from EELS-FEI Company provided with a 300 kV emission gun and 1 Å line resolution, coupled with HAADF and EDAX modules.

SEM imaging

For cross-sectional microscopic evaluation, each specimen was fractured in liquid nitrogen and gold sputtered thereafter, in order to avoid superficial charging under the electron beam. Morphological studies were done on a QUANTA INSPECT F scanning electron microscope (SEM) from FEG-FEI Company, equipped with a field emission gun of 1.2 nm resolution and an energy dispersive X-ray spectrometer module with 133 eV, Mn Kα resolution.

MicroCT analysis

Parallelepiped specimens (~2 mm length and width and ~3 mm height) were harvested from the middle region of each sample and subsequently treated with an ethanol-based iodine solution (1.5 wt.%, 24 h immersion) in order to enhance X-ray absorption. Prior to microCT scanning, samples structures were fixed by immersion in hexamethyldisilazane for 3 hours, followed by air drying overnight.

A Bruker microCT 1172 high-resolution equipment (N.V., Kontich, Belgium) was used for microCT analysis. The source voltage and current were set to 50 kV and 199 µA, respectively, with a total power of 10 W, whereas no filter was used. The voxel resolution was set to 0.68 µm. Each sample was rotated to 360˚, with a rotation angle of 0.34 ˚ and 5 average frames per capture. Raw data reconstruction to sequential tomograms was made using NRecon 1.6.10.1 reconstruction software from Bruker microCT. The ring artefact reduction was set to 10, beam hardening correction was 20, and smoothing was 1. For each sample, a number of 4 VOI datasets with the same dimensions was extracted using CTAn 1.14.4.1+ (Bruker microCT). 3D volumes were saved using CTVox 3.0.0 r1114 software from Bruker microCT. 3D analysis of the VOIs involved the creation of a task list which consisted of thresholding, despeckling and 3D analysis, with no supplementary image processing. The reported numerical results represent average values of 4 measurements per sample with standard deviation (± S.D.).

Compressive tests

In advance of mechanical testing, a number of 10 cylindrical specimens with ~6 mm diameter and ~6 mm height was prepared for each sample. Specimens were cut from samples middle region and tested thereafter by vertical unidirectional compressive load, using a Zwick (ZwickRoell, Ulm, Germany) mechanical tester. A 0.5 N preload force was set at speed of 10 mm / minute, while testing was made with 0.5 mm / second along the vertical axe, after the preload was reached. Testing was performed in samples dry state, at room temperature. Compressive strength at 10 % indentation travel and Young's modulus are reported as the average values of 10 measurements ± S.D.

Young's modulus (E) was calculated from the obtained data using the following formula:

$$E = \Delta\varepsilon\,\Delta\sigma^{-1}, \tag{3}$$

where Δε and Δσ represent the variation of compressive strain (ε) and strength (σ), respectively, calculated in the linear curve region, from ε = 1 % to ε = 2 %.

Biocompatibility assessments

PVA-Gel-GO 3D scaffolds were subjected to sterilization by exposure to UV for 30 minutes on each side, to exclude the possibility of infection when put in contact with the cellular component. The dried scaffolds were then inflated for 24 hours in cell culture media, to allow the 3D structure to stabilize in liquid media and also to wash the possible debris from synthesizing procedure. Processed Gel – PVA / GO scaffolds were then tested for biological activity and cytotoxicity by a set of indirect cytocompatibility tests. Considering that these GO-containing materials have been synthesized particularly for bone tissue engineering applications and bone regeneration purposes, their cytocompatibility was tested on murine preosteoblasts from MC3T3-E1 cell line.

After 24 hours of washing, each Gel – PVA / GO 0.5-3 wt.% composition was immersed and maintained in 3 mL of fresh cell culture media for another 24 hours, in standard conditions of culture (5% CO_2, 37 °C, adequate humidity). The extracts obtained for each composition were harvested and used as samples to test the cytotoxic potential *versus* preosteoblasts.

Cells were seeded in 24-well plates using an initial density of 1.5×10^4 cells/cm^2 and they were allowed to reach approx. 80% confluence (using standard culture conditions) before they were exposed to scaffold extracts.

Once the cells acquired the required density and phenotype, they were put in contact with the scaffold extracts. Triplicate wells seeded with preosteoblasts were used for each scaffold composition extract. In order to evaluate the cytotoxic potential of the materials, untreated preosteoblasts cultured in normal media served as reference (control).

After 24 hours of contact, levels of lactate dehydrogenase (LDH) released in the cell culture media by the cells exposed to the extracts were measured as sign of the possible cytotoxic effects of Gel – PVA / GO scaffolds. Simultaneously, MTT assay was performed in order to assess preosteoblasts viability after 24 h of contact with the released extracts. MTT and LDH assays were performed following manufacturer's instructions and the results were measured spectrophotometrically at 550 nm and 490 nm, respectively.

Statistical analysis

For microCT 3D analysis and compressive testing, the obtained mean values ± S.D were compared by Holm-Sidak all pairwise multiple comparison method (one-way ANOVA), using SigmaPlot v.13 software (Systat Inc, St. Louis, USA). Differences of $p \leq 0.05$ between compared groups were considered statistically significant. For biological tests, data were normalized to the values obtained during MTT and LDH assays for untreated cells and were statistically analyzed using one-way ANOVA method followed by Bonferroni's multiple comparison test. The results were expressed as a mean ± S.D. using GraphPad Prism Software.

Results and discussion

FT-IR

FT-IR spectrometry was employed for materials structural characterization at the molecular level. Considering the present case, such particularities are of high interest, as our samples physical-chemical outcomes will depend on how Gel - PVA, Gel - GO and PVA – GO interact. FT-IR spectra of Gel - PVA illustrated in Fig. 1 A comprises the characteristic absorption bands of both Gel and PVA. The broad band expanding in the 3000 to 3600 cm^{-1} range is related to OH bending. Two small peaks are generated around 2939 and 2912 cm^{-1}, being attributed to CH asymmetric and symmetric stretching vibration. CH vibration also generates the band at 1330 cm^{-1}. The secondary structure of Gel is highlighted by the specific bands of amides I, II and III, generated at 1656-1640, ~1547 and ~1238 cm^{-1}.[33, 34] Amides A and B of Gel usually occur around 3325 and 2925 cm^{-1}, thus one may consider the overlapping of these bands with the OH and CH region, respectively.[35] Peaks provided by PVA are recorded at 1143 and 1092 cm^{-1} and are attributed to C-O groups of the ordered and amorphous regions of PVA [36] and their intensity ratio is often used to evaluate the degree of PVA structural order. In addition, the two small bands found at 921 and 854 cm^{-1} were generated by the stretching vibration of C-C bonds.[37]

With the addition of GO (Fig. 1 B-E), the Amide I vibrational stretch band of Gel splits into two partially overlapped bands. Here, the band from 1656 cm^{-1} suggests the presence of α-helical regions, while the β-sheets express near 1640 cm^{-1}, suggesting a rearrangement of Gel secondary structure. A more pronounced decrease of the β-sheets band was observed with the addition of GO, for which I_{1656}/I_{1640} ratio decreased from 1.03 to 0.91. The process of Gel renaturation is known to take place during cooling processes and is mainly governed by H bonding.[38, 39] However, in this case it seems that GO is the main factor to promote the reorganization of Gel random coils to triple helical domains. Furthermore, the band of Amide II almost doubles its intensity with the addition of 0.5 - 3 wt.% GO, while it is shifted from 1547 to 1536 cm^{-1} for 2 and 3 wt.% GO concentrations. This phenomenon is known to occur when intermolecular H interactions are facilitated.[33] Another change due to GO incorporation is the progressive decrease of the OH in plane wagging band at 1443 cm^{-1}, whose intensity decreases to almost a third. Along with the reduction of OH broad band around 3000-3600 cm^{-1}, this change might be another indication of H bonding, supported by the existence of reactive functional groups of the three components, especially from PVA multiple OH groups.[40] The most important feature is the absence of the Gel typical peak usually occurred around 1680 cm^{-1}, which is an indication that most of the –COOH groups of Gel were esterified,[41] in reaction with –OH groups of both PVA and GO. Regarding GO influence on PVA, an increased value of the ordered *vs.* amorphous bands was observed (Table 1), suggesting a more ordered arrangement of PVA chains possibly under the guidance of GO sheets.[36] The highest ratio value was obtained for the composite containing 0.5 wt.% GO, with a I_{1143}/I_{1092} increase from 0.563 to 0.653.

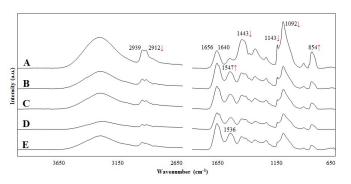Journal of Materials Chemistry B   **ARTICLE**

Fig. 1 FT-IR spectra of Gel – PVA (A) and Gel – PVA / GO biocomposites with 0.5, 1, 2 and 3 wt.% GO (B-E).

Based on the obtained results, we assume that GO set interactions with both Gel and PVA molecules. On the one hand, –COOH groups of Gel are esterified by –OH groups of PVA and GO, while those of GO are esterified by –OH groups of PVA. On the other hand, multiple H bonds are created during Gel renaturation, while it is well known that PVA chains highly react to one another by H bonds. Therefore, we expect a polymer-GO mixture, where GO nanosheets interact with the polymeric domains which in turn are found in both random and organized states.

XRD

Keeping in mind the idea that a more ordered structure leads to better material stability, the evaluation of structural arrangement is of great importance for biomaterials characterization. In this regard, XRD analysis gives an overview of structural arrangements by providing information about the amorphous and ordered domains within materials. X-ray diffractograms of the obtained materials are illustrated in Fig. 2 and correlated data are listed in Table 1, columns 3 to 6. The peak generated around $2\vartheta \sim 11$ ° in Fig. 2 A reflects the (002) organization of GO lattices which, according to Bragg's law, yields a d-spacing of 8.03 Å.[42] This value fits within the typical values of GO nanosheets separation, known to range from 6 to 12 Å, as a result of the functionalization degree.[43] The Bragg reflection identified at 19.8 ° in Gel – PVA spectrum (Fig. 2 B) is assigned to d = 4.46 Å and τ = 13.5 Å.
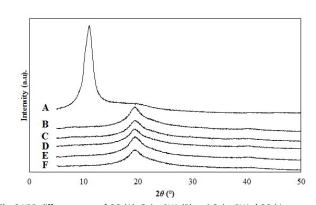
On the one hand, this band emphasizes the existence of PVA crystalline arrangement under (101) monoclinic form, while the amorphous PVA phase generates the weak band at 42.7 °.[44, 45] On the other hand, Gel is also known to express its ordered structuration around 2ϑ = 20 °.[46] Therefore we assigned the peak from this region to be a sum of the signals generated by the ordered assembling of both PVA and Gel chains.

With the addition of GO, the decrease of FWHM calculated for this band indicates an upturn of τ values (Table 1, column 6). Among all concentrations, 0.5 wt.% GO proved to be the favorable one, with a τ increase from 13.5 to 18.2 Å. This phenomenon indicates GO nanosheets possibility to react in a synergic way with the polymeric chains and towards a more ordered structuration.[40] The idea is also supported by FT-IR indications regarding Gel chains reorganization and also by PVA enhanced crystallinity, while a good dispersion of oxygenated graphene small amounts within composites is suggested by the absence of GO specific peak from the composites spectra.

TEM

In order to visualize the dispersion degree of GO nanosheets within polymeric matrix and to emphasize on several microporosity related aspects, materials structuration was investigated by TEM. Fig. 3 displays the intrinsic characteristics of the Gel-PVA composite containing 0.5 wt.% GO. According to Fig. 3 A, GO layers composed by few nanosheets are efficiently dispersed within Gel – PVA phase and seem to be arranged in a distinctive manner along the polymers walls. A more detailed view of GO flakes flexibility and their orientation along polymer structures is supported by the higher magnification TEM micrograph displayed in Fig. 3 B, where the arrows point out few GO nanosheets bent together.

High resolution TEM imaging can offer some indications about GO sheets packing mode,[47] *i.e.* turbostratic (parallel), Bernal (ABA) or rhomboedric (ABC), among which ABA configuration is indicated to be stable and typical for exfoliated materials.[48] However in the present case it is difficult to appreciate such features by direct TEM visualization and we must also take into consideration the following arguments.

Table 1 Ordered *vs.* amorphous domains of PVA expressed as the ratio of their corresponding FT-IR bands intensities (I_{1143} / I_{1092}) and XRD measurements of d-spacing, FWHM and τ assigned to the 19.88 - 19.60 ° bands.

Sample	I_{1143} / I_{1092}	2ϑ (°)	d-spacing (nm)	FWHM (°)	τ (Å)
Gel - PVA	0.563	19.88	4.46	4.30	13.50
Gel - PVA / GO 0.5 wt.%	0.653	19.60	4.52	3.19	18.20
Gel - PVA / GO 1 wt.%	0.619	19.70	4.50	3.80	15.30
Gel - PVA / GO 2 wt.%	0.633	19.80	4.49	3.43	16.98
Gel - PVA / GO 3 wt.%	0.594	19.70	4.50	3.51	16.54

Fig. 2 XRD diffractograms of GO (A), Gel – PVA (B) and Gel – PVA / GO biocomposites with 0.5, 1, 2 and 3 wt.% GO (C-F).
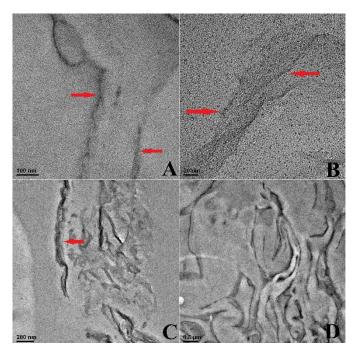
ARTICLE

Fig. 3 TEM images of 0.5 wt.% containing Gel – PVA / GO composite. Scale bars are 100 nm (A), 20 nm (B), 200 nm (C) and 0.5 μm (D).
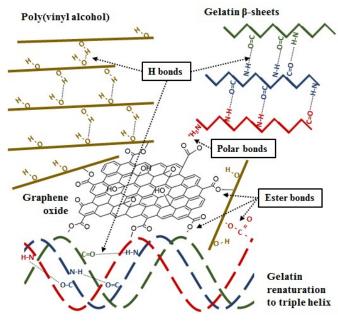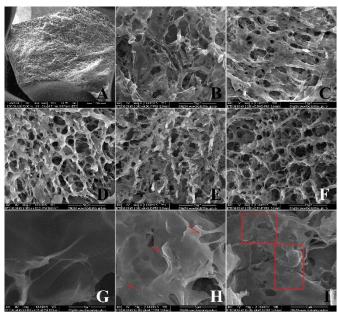

Fig. 4 Schematic view of the proposed structuration model for Gel – PVA / GO composite scaffolds.

Even though good GO dispersions can be achieved through sonication, some studies report nanosheets disruption into smaller sheets under the US stress.[21] In addition, sheets packing depend on the interactions between GO functional groups, which are known to be randomly distributed onto the carbon structure.[49] It is therefore difficult to appreciate an overlapping model for GO nanosheets and we consider that ABA could be the GO stacking model more likely to occur within the Gel – PVA / GO composite materials. Conversely, only seldom agglomerates similar to the alternate GO layers pointed by the arrow in Fig. 3 C were visualized throughout the polymers phase. In addition, TEM provides information about biomaterials inner pore architectures. Along with macro-porosity, micro-porosity plays critical roles for some biological activities, for instance in biomineralization and osteoinduction or for the transplantation of sensitive tissues such as the extrahepatic isles.[50-52] Fig. 3 D confirms the existence of irregular interconnected micropores, here visualized in the vertical sectioning of 0.5 wt.% GO containing scaffold. Subsequently, macro-pores characterization will be discussed in detail within the next sections. Along with FT-IR and XRD indications, TEM provides complementary information to validate the development of a unique structuration pattern under the influence of GO incorporation. Accordingly, the three components interact mainly through ester and H bonding. In addition to the amorphous phases, both the polymers and the GO nanosheets are also found in more ordered arrangements, *i.e.* Gel in the helical orientation, PVA in linearly arranged chains and GO as few packed nanosheets. Therefore we propose the following model (Fig. 4) as a main structuration pattern for Gel – PVA / GO composite scaffolds.

SEM

Freeze-dried scaffolds morphologies vary along vertical direction, being mainly determined by the orientation of ice crystals size and orientation, which in turn depend on freezing temperature, rate and time.[53, 54] A representative cross-sectional SEM micrograph of our samples is displayed in Fig. 5 A, revealing the variation of pore architecture from top (air side) to bottom (dish side). Middle regions were chosen for further comparison of unloaded *vs.* GO loaded samples.

A good compatibility of Gel, PVA and GO could be observed for all the composites, for which the three components are seen completely dissolved and fused altogether into random oriented structures, without obvious phase separation. All materials display a foam-like appearance, with irregular interconnected pores walled by wrinkled composite structures (Fig. 5 B-F). Pore sizes vary from few to several tens of μm, while seldom pores of hundreds nm size could be observed at higher magnification (figures not shown). However, an apparent difference between Gel - PVA and Gel - PVA / GO composite scaffolds was observed. The cross-section micrograph of GO - free scaffold reveals undefined pore shapes, with smooth and thick pore walls. A more homogenous architecture is formed with the progressive incorporation of GO within polymer matrix, leading to thinner yet more crumpled pore walls at the same time. By further high SEM magnification, sharp prominences were identified onto the pore walls of GO containing scaffolds (Fig. 5 H and I). Their absence from Gel – PVA micrographs (Fig. 5 G) match TEM indications, supporting the presence of GO nanosheets at the polymeric surfaces. Such structures can play important roles particularly for mechanical behavior and biological activities.
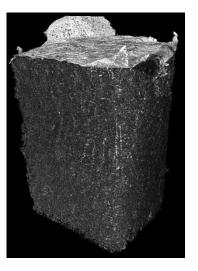
Fig. 5 Overall morphology imaged by SEM for Gel – PVA (A) displayed at 1 mm scale. SEM micrographs of Gel – PVA (B) and Gel – PVA / GO composites containing 0.5, 1, 2 and 3 wt.% (C-F). GO prominences present onto the pore walls of 2 wt.% composite (H and I) and their absence from Gel – PVA scaffold (G). Scale bars are 50 μm (B-F) and 5 μm (G-I).

Fig. 6 Cross-sectional view of the overall morphological variation and the formation of the top layer, evidenced through microCT 3D rendering of a random volume of Gel – PVA composite.

On the one hand, it was shown that GO nanosheets can receive and transfer mechanical loads in a more facile way within polymers [55], while on the other hand carbon-based materials can strongly attach cells and facilitate the development of more focal adhesions.[24, 56] In the view of such considerations, plus the structural homogenization observed by SEM, we presume that GO will provide better compressive resistance for our biopolymer composites and offer a biocompatible environment able to sustain cellular activities.

MicroCT

Fig. 6 illustrates the 3D rendering of a random Gel - PVA volume, aimed to give a general view of our materials construction mode. A thin dense layer is formed on top of the samples, beneath which samples are highly porous and anisotropic. Likewise for SEM studies, further characterization was focused on the middle region of the composites, since this layer can induce artefacts in terms of microCT 3D analysis, mechanical tests and biocompatibility assessments. 3D analysis indicated all samples to have anisotropic structures, with less than 0.1 % closed pores related to the total volume. Table 2 reports the average values of total porosity, structures thickness and specific surface. A correlation between 0.5 and 3 wt.%, as well as between 1 and 2 wt.% GO concentrations was highlighted for all the 3D analysis results. For instance, the total porosity tends to decrease from 62 % to 51 % and 43 % for 0.5 and 3 wt.% GO, respectively. At the same time, increased values are obtained for the other two concentrations. Expressed as the ratio of object surface per object volume, the specific surface goes hand in hand with the pores percentage, following a similar variation with the GO concentration.

Table 2 Total porosity (Po(tot)), structures thickness (St.Th.) and specific surface (Obj.S / Obj.V) reported as average values of 3D analysis measurements for 4 distinct VOIs with the same size per sample.

Sample	Po(tot) (%)	St.Th.(μ)	Obj.S / Obj.V (1/μ)
Gel - PVA	62 ± 1.75[1]	7.59 ± 0.21[3,4]	0.476 ± 0.018[6]
Gel - PVA / GO 0.5 wt.%	51 ± 4.26	7.85 ± 0.54[3]	0.443 ± 0.040[6]
Gel – PVA / GO 1 wt.%	64 ± 0.99[1,2]	6.98 ± 0.24[4,5]	0.539 ± 0.016
Gel - PVA / GO 2 wt.%	69 ± 1.96[2]	6.29 ± 0.21[5]	0.611 ± 0.025
Gel – PVA / GO 3 wt.%	43 ± 3.75	8.83 ± 0.64	0.377 ± 0.034

[1-5] insignificant differences between the marked values by statistical analysis ($p < 0.05$).

The structure thickness (St.Th.) is expressed as the mean thickness of all objects, i.e. the average thickness of material walls and it can offer some predictions on materials mechanical stability. The slight St.Th. increase occurred at low GO concentration is not statistically significant compared to control, while a significant increase was recorded in the case of 3 wt.% GO. The thinnest material structures were indicated to be developed with the addition of 1 and 2 wt.% GO. Yet the microCT method used in this study is limited when considering micro-porosities formerly evidenced through TEM investigation. Keeping in mind the tradeoff between the need of contrast agent staining and materials preservation, we can consider our microCT analysis method as reliable for providing consistent data with reference to the parameters here reported. Fig. 7 offers an overall view of cross-sectional SEM micrographs, microCT tomograms and microCT 3D renderings
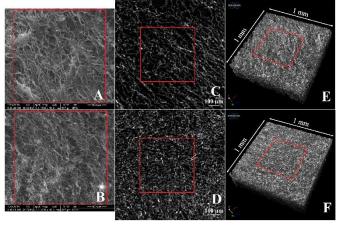
Fig. 7 Comparative view between unloaded and 0.5 wt.% GO loaded composites through SEM images (A and B), microCT tomograms (C and D) and VOIs 3D rendering (E and F). Scale bars are 100 μm for fig. A - D. The red squares frame areas of 500 μm.

Table 3 Compressive strength (σ) at 10 % indentation travel, Young's Modulus (E) and their percent of increase with the addition of GO (values reported as averages of 10 measurements per sample ± S.D.).

Sample	σ (MPa)	σ * (%) increase	E (MPa)	E * (%) increase
Gel – PVA	0.111 ± 0.026	-	0.012 ± 0.005[2]	-
Gel - PVA / GO 0.5 wt.%	0.219 ± 0.049[1]	97	0.020 ± 0.008[2,3]	67
Gel - PVA / GO 1 wt.%	0.221 ± 0.021[1]	99	0.025 ± 0.007[3]	108
Gel - PVA / GO 2 wt.%	0.226 ± 0.031[1]	104	0.026 ± 0.007[3]	117
Gel - PVA / GO 3 wt.%	0.233 ± 0.022[1]	110	0.028 ± 0.008[3]	133

*increase related to Gel – PVA (control sample). [1-3] insignificant differences between the marked values by statistical analysis ($p < 0.05$).

of Gel – PVA / GO 0.5 wt.% in comparison with Gel – PVA control. Here, morphological observations confirm the pores homogenizing under the addition of GO, previously suggested by SEM studies.

Compressive mechanical testing

While numerous studies declare pristine graphene (G) as the strongest material ever measured,[57, 58] atomistic calculations prove that G sheets with numerous defects and wide slope boundaries have similar strengths as the defect-free material.[59] Therefore, G derivatives are also expected to have superior mechanical properties and improve materials resistance against mechanical stress. Considering the aimed applications, GO capacity to reinforce Gel – PVA composites was evaluated by compressive mechanical testing. For each sample, a number of 10 cylindrical specimens with same diameter and height were cut and compressed at a speed of 0.5 mm / min. Extracted data were processed and results are visualized in Fig. 8 and Table 3.
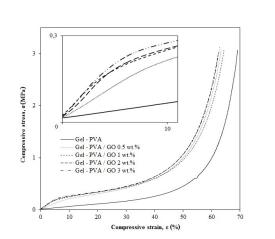

Fig. 8 Graphical representation illustrating the mechanical response of Gel - PVA and Gel – PVA / GO spongious composites against compressive stress.

All composite curves follow the smooth characteristic pattern of an elastomer compression,[60] displaying the three specific regions of *i*. elastic bending (initial linear segment), *ii*. plastic deformation (plateau) and *iii*. final densification. Subsequently, both graphical representation and tabulated data confirm the beneficial effect of GO incorporation within the polymer blending. At 10 % indentation travel during elastic deformation, compressive strength was improved by 97 - 110 % with the addition of 0.5 - 3 wt.% GO. As a result, GO containing scaffolds reach the same compressive strengths at earlier indentation travels, which in turn indicates less deformation and enhanced materials rigidity. Moreover, mechanical behavior patterns are kept throughout the entire testing, with an overall improvement of ~ 2 times of both compressive strength and elastic modulus. Reported values support the idea that the addition of GO sheets can increase polymer composites stiffness and act as reinforcing agents towards compressive stress. Though no statistical significant differences were observed by comparing the four GO amounts, one should take into account the great effect that GO incorporation can induce in polymer composites, even at such low concentrations. Another explanation could be drawn on the basis of Gel chains helical reorganizing in the presence of GO, as well as on the enhanced crystallinity of PVA domains, both shown by FT-IR and XRD. Along with the porosity homogenization, such conformational changes were probably the main mechanism to provide higher mechanical stability for Gel – PVA / GO composite scaffolds.

Biocompatibility tests

The MTT assay was performed to check preosteoblasts metabolic activity after contact with Gel – PVA / GO extracts, as compared to the viability of the untreated cells used as control. MTT assay results showed a generally good cytocompatibility of the Gel – PVA / GO scaffolds with preosteoblasts (Fig. 9 A), with percentages of viability comparable to control viability. No statistically significant differences were detected in viability for cells exposed to Gel – PVA scaffold and the cells treated with

Gel - PVA / GO 0.5 and 1 wt.%, suggesting that the addition of small amounts of GO in scaffolds composition has limited or undetectable effect upon preosteoblasts viability throughout 24 hour of in vitro assay.

Notably, extracts harvested from Gel - PVA / GO 2 and 3 wt.% significantly influenced cell viability (p<0.05), which confirms GO positive effect on cell viability and proliferation. Our group has previously stated the same favoring effect of GO on the interaction between the cellular component and GO-containing composites (chitosan - GO, chitosan / PVA - GO, polysulfone - GO).[19, 22, 61]

Gel - PVA / GO 0.5-3 wt.% composites cytotoxic potential was evaluated proportionally to the levels of LDH released in the culture media by the cells with a damaged membrane after cell exposure to composite scaffolds extracts (Fig. 9 B). LDH assay results revealed a statistically higher cytotoxicity (p < 0.05) on preosteoblasts for all tested extracts, as compared to the LDH levels detected in control untreated culture. These differences are considered basal levels of cytotoxicity due to the influence exerted by the materials chemical composition on cellular processes. No statistically significant increases in cytotoxicity were observed for cells exposed to Gel - PVA / GO 0.5 - 3 wt.% extracts, as compared to the preosteoblasts treated with Gel – PVA extract, suggesting that the presence of GO in the composition of these materials exhibits no particular influence on the cytotoxicity of the scaffolds *versus* preosteoblasts. In this context, the detected levels of cytotoxicity are probably due to the general chemical composition of the scaffolds and to the association of synthetic components to the gelatin base in order to optimize the mechanical properties and porosity of the materials.
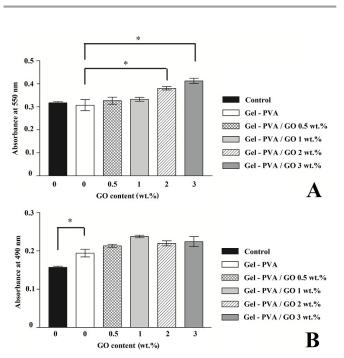

Fig. 9 Preosteoblasts viability assessed after 24 h contact with PVA - Gel / GO 0.5 - 3 wt.% composites extracts by MTT assay (A). PVA – Gel / GO 0.5 - 3 wt.% composites cytotoxic potential exerted on preosteoblasts after 24 h of indirect contact, as revealed by LDH assay (B). *significant differences by statistical analysis (p<0.05).

Conclusions

New Gel – PVA / GO composite biomaterials with 0.5 – 3 wt.% GO were synthesized and physically cross-linked through freeze-thawing techniques. Characterization included structural evaluation, bidimensional and tridimensional features analysis, mechanical tests and biocompatibility assessments.

FT-IR results suggested the settlement of cohesive interactions between the three components of our biocomposite system, *i.e.* Gel, PVA and GO, governed by esterification and H bonds formation. Together with XRD indications, a more ordered structuration of composite materials was observed with the addition of GO. TEM supported the idea of efficient GO dispersion within polymer matrix and, along with SEM and microCT results, confirmed the development of highly porous materials, with both macro- and micro-porosities. Compressive tests demonstrated once again the potential of GO to enhance mechanical features of polymeric scaffolds. As a result, compressive strength of Gel – PVA biomaterials was doubled under the influence of 0.5 - 3 wt.% GO incorporation. Eventually, our materials showed low cytotoxicity and were able to sustain murine preosteoblasts viability. Amongst the obtained biomaterials, the composite with 0.5 wt.% GO was indicated to exhibit the most promising features, for which FT-IR indicated the highest degree of PVA chain crystallinity, while the mean size of the ordered domains extracted by XRD was also found to increase the most. Moreover, GO nanosheets arrangement within the polymeric matrix was evidenced through TEM and SEM altogether. MicroCT studies supported SEM results and confirmed the development of smoother pores. In terms of mechanical resistance, the addition of 0.5 wt.% GO increased Gel – PVA compressive strength by 97 %, from 0.111 MPa to 0.219 MPa. In addition, the optimized combinations of naturally occurring Gel, synthetically derived PVA and GO, allowed for equilibrated preosteoblasts cellular activities.

In conclusion, the newly obtained Gel – PVA / GO composite system meets several prerequisites for the development of hard tissue engineering scaffolds, for instance well-determined structures, porous architectures and improved mechanical performances, along with the indispensable low cytotoxicity. Therefore Gel – PVA / GO can be recommended for further *in vivo* testing, opening new prospects for the development of both hard and soft tissue engineering applications.

Acknowledgements

References

1. D. W. Hutmacher, *Biomaterials*, 2000, **21**, 2529-2543.
2. M. A. M. Dorothee Rickert, A.Lendlein, S.Kelch, R.-P. Franke, *Clinical Hemorheology and Microcirculation*, 2003, **28**, 175–181.
3. E. A. C. Thomas H. Petersen, Liping Zhao, Eun Jung Lee, Liqiong Gui, MichaSam B. Raredon, Kseniya Gavrilov, Tai Yi, Zhen W. Zhuang, Christopher Breuer, Erica Herzog, Laura E. Niklason, *Science*, 2010, **329**, 538-541.
4. A. Sionkowska, *Progress in Polymer Science*, 2011, **36**, 1254-1276.
5. F. A. M. Alizadeh, A.B. Khoshfetrat, H. Ghaleh, *Materials Science and Engineering C*, 2013, **33**, 3958–3967.
6. M. Achilli and D. Mantovani, *Polymers*, 2010, **2**, 664.
7. M. Mozafari, M. Rabiee, M. Azami and S. Maleknia, *Applied Surface Science*, 2010, **257**, 1740-1749.
8. A. K. M. M. A. Quazi T.H. Shubhra, M.D.H. Beg, *Materials Letters*, 2011, **65**, 333-336.
9. X. T. Shiv Shankar, Gaobin Li, Jong-Whan Rhim, *Food Hydrocolloids*, 2015, **45**, 264e271.
10. N. S. C. Kailasanathan, Vasant Naidu, *Ceramics International*, 2012, **38**, 571–579.
11. D. Zhang, W. Zhou, B. Wei, X. Wang, R. Tang, J. Nie and J. Wang, *Carbohydrate Polymers*, 2015, **125**, 189-199.
12. M. I. Baker, S. P. Walsh, Z. Schwartz and B. D. Boyan, *Journal of Biomedical Materials Research Part B: Applied Biomaterials*, 2012, **100B**, 1451-1457.
13. S. Nkhwa, K. F. Lauriaga, E. Kemal and S. Deb, *Conference Papers in Science*, 2014, **2014**, 7.
14. A. S. Asran, S. Henning and G. H. Michler, *Polymer*, 2010, **51**, 868-876.
15. N. Alexandre, J. Ribeiro, A. Gärtner, T. Pereira, I. Amorim, J. Fragoso, A. Lopes, J. Fernandes, E. Costa, A. Santos-Silva, M. Rodrigues, J. D. Santos, A. C. Maurício and A. L. Luís, *Journal of Biomedical Materials Research Part A*, 2014, **102**, 4262-4275.
16. V. Karageorgiou and D. Kaplan, *Biomaterials*, 2005, **26**, 5474-5491.
17. S. Panzavolta, B. Bracci, C. Gualandi, M. L. Focarete, E. Treossi, K. Kouroupis-Agalou, K. Rubini, F. Bosia, L. Brely, N. M. Pugno, V. Palermo and A. Bigi, *Carbon*, 2014, **78**, 566-577.
18. M. A. Rafiee, J. Rafiee, Z. Wang, H. Song, Z.-Z. Yu and N. Koratkar, *ACS Nano*, 2009, **3**, 3884-3890.
19. M. Ionita, A. M. Pandele, L. Crica, S. Dinescu, M. Costache, H. Iovu, *Carbohydrate Polymers*, 2014, **102**, 813– 820.
20. K. S. Novoselov, V. I. Falko, L. Colombo, P. R. Gellert, M. G. Schwab and K. Kim, *Nature*, 2012, **490**, 192-200.
21. D. R. Dreyer, S. Park, C. W. Bielawski and R. S. Ruoff, *Chemical Society Reviews*, 2010, **39**, 228-240.
22. S. Dinescu, M. Ionita, A. M. Pandele, B. Galateanu, H. Iovu, A. Ardelean, M. Costache and A. Hermenean, *Bio-medical materials and engineering*, 2014, **24**, 2249-2256.
23. S. Shadlou, B. Ahmadi-Moghadam and F. Taheri, *Materials & Design*, 2014, **59**, 439-447.
24. L. Feng, L. Wu and X. Qu, *Advanced Materials*, 2013, **25**, 168-186.
25. T. R. Nayak, H. Andersen, V. S. Makam, C. Khaw, S. Bae, X. Xu, P.-L. R. Ee, J.-H. Ahn, B. H. Hong, G. Pastorin and B. Özyilmaz, *ACS Nano*, 2011, **5**, 4670-4678.
26. W. C. Lee, C. H. Y. X. Lim, H. Shi, L. A. L. Tang, Y. Wang, C. T. Lim and K. P. Loh, *ACS Nano*, 2011, **5**, 7334-7341.
27. M. Fiorillo, A. F. Verre, M. Iliut, M. Peiris-Pagés, B. Ozsvari, R. Gandara, A. R. Cappello, F. Sotgia, A. Vijayaraghavan and M. P. Lisanti, *Graphene oxide selectively targets cancer stem cells, across multiple tumor types: Implications for non-toxic cancer treatment, via "differentiation-based nano-therapy"*, 2015.
28. B. S. Bhatnagar, R. H. Bogner and M. J. Pikal, *Pharmaceutical development and technology*, 2007, **12**, 505-523.
29. M. H. Lee, M. H. Baek, D. S. Cha, H. J. Park and S. T. Lim, *Food Hydrocolloids*, 2002, **16**, 345-352.
30. W. S. Hummers, & Offeman, R. E. (1958), *Journal ofAmerican Chemical Society*, **80**, 1339.
31. C. G. Pope, *Journal of Chemical Education*, 1997, **74**, 129.
32. U. Holzwarth and N. Gibson, *Nat Nano*, 2011, **6**, 534-534.
33. J. H. Muyonga, C. G. B. Cole and K. G. Duodu, *Food Chemistry*, 2004, **86**, 325-332.
34. G. Al-Saidi, A. Al-Alawi, M. Rahman and N. Guizani, *International Food Research Journal*, 2012, **19**, 1167-1173.
35. P. Tongnuanchan, S. Benjakul and T. Prodpran, *Food Chemistry*, 2012, **134**, 1571-1579.
36. H. J. Salavagione, M. A. Gómez and G. Martínez, *Macromolecules*, 2009, **42**, 6331-6334.
37. M. Miya, R. Iwamoto and S. Mima, *Journal of Polymer Science: Polymer Physics Edition*, 1984, **22**, 1149-1151.
38. M. Roussenova, J. Enrione, P. Diaz-Calderon, A. J. Taylor, J. Ubbink and M. A. Alam, *New Journal of Physics*, 2012, **14**, 035016.
39. Y. Ohyabu, S. Yunoki, H. Hatayama and Y. Teranishi, *International Journal of Biological Macromolecules*, 2013, **62**, 296-303.
40. Y. He, N. Zhang, Q. Gong, H. Qiu, W. Wang, Y. Liu and J. Gao, *Carbohydrate Polymers*, 2012, **88**, 1100-1108.
41. K. Pal, A. K. Banthia and D. K. Majumdar, *Aaps Pharmscitech*, 2007, **8**, E142-E146.
42. H.-K. Jeong, Y. P. Lee, R. J. W. E. Lahaye, M.-H. Park, K. H. An, I. J. Kim, C.-W. Yang, C. Y. Park, R. S. Ruoff and Y. H. Lee, *Journal of the American Chemical Society*, 2008, **130**, 1362-1366.
43. S. Stankovich, D. A. Dikin, R. D. Piner, K. A. Kohlhaas, A. Kleinhammes, Y. Jia, Y. Wu, S. T. Nguyen and R. S. Ruoff, *Carbon*, 2007, **45**, 1558-1565.
44. O. Okay, *Polymeric Cryogels: Macroporous Gels with Remarkable Properties*, Springer International Publishing, 2014.
45. R. Ricciardi, F. Auriemma, C. De Rosa and F. Lauprêtre, *Macromolecules*, 2004, **37**, 1921-1927.
46. K. Pal, A. K. Banthia and D. K. Majumdar, *Journal of Biomaterials Applications*, 2006, **21**, 75-91.
47. C. Gómez-Navarro, J. C. Meyer, R. S. Sundaram, A. Chuvilin, S. Kurasch, M. Burghard, K. Kern and U. Kaiser, *Nano Letters*, 2010, **10**, 1144-1148.
48. C. H. Lui, Z. Li, Z. Chen, P. V. Klimov, L. E. Brus and T. F. Heinz, *Nano Letters*, 2011, **11**, 164-169.
49. D. A. Dikin, S. Stankovich, E. J. Zimney, R. D. Piner, G. H. Dommett, G. Evmenenko, S. T. Nguyen and R. S. Ruoff, *Nature*, 2007, **448**, 457-460.
50. D. Le Nihouannen, G. Daculsi, A. Saffarzadeh, O. Gauthier, S. Delplace, P. Pilet and P. Layrolle, *Bone*, 2005, **36**, 1086-1093.
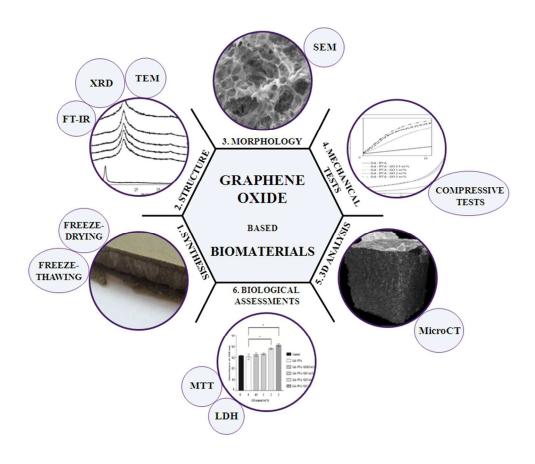
ARTICLE

51. S. Fujibayashi, M. Neo, H.-M. Kim, T. Kokubo and T. Nakamura, *Biomaterials*, 2004, **25**, 443-450.
52. R. F. Gibly, X. Zhang, M. L. Graham, B. J. Hering, D. B. Kaufman, W. L. Lowe, Jr. and L. D. Shea, *Biomaterials*, 2011, **32**, 9677-9684.
53. F. J. O'Brien, B. A. Harley, I. V. Yannas and L. Gibson, *Biomaterials*, 2004, **25**, 1077-1086.
54. J. Zhang, A. Zhou, A. Deng, Y. Yang, L. Gao, Z. Zhong and S. Yang, *Materials Science and Engineering: C*, 2015, **49**, 174-182.
55. M. Ionita, A. M. Pandele, L. Crica and L. Pilan, *Composites Part B: Engineering*, 2014, **59**, 133-139.
56. S.-R. Ryoo, Y.-K. Kim, M.-H. Kim and D.-H. Min, *ACS Nano*, 2010, **4**, 6587-6598.
57. C. Lee, X. Wei, J. W. Kysar and J. Hone, *Science*, 2008, **321**, 385-388.
58. S. Stankovich, D. A. Dikin, G. H. B. Dommett, K. M. Kohlhaas, E. J. Zimney, E. A. Stach, R. D. Piner, S. T. Nguyen and R. S. Ruoff, *Nature*, 2006, **442**, 282-286.
59. R. Grantab, V. B. Shenoy and R. S. Ruoff, *Science*, 2010, **330**, 946-948.
60. T. H. Courtney, *Mechanical Behavior of Materials*, McGraw-Hill International Editions, 2000
61. M. Ionita, E. Vasile, L. E. Crica, S. I. Voicu, A. M. Pandele, S. Dinescu, L. Predoiu, B. Galateanu, A. Hermenean and M. Costache, *Composites Part B: Engineering*, 2015, **72**, 108-115.

237x195mm (96 x 96 DPI)